Computer-Aided Civil and Infrastructure Engineering 43 (2026) 100028

Contents lists available at ScienceDirect

Computer-Aided Civil and Infrastructure Engineering

journal homepage: www.sciencedirect.com/journal/computer-aided-civil-and-infrastructure-engineering

Research article

A lightweight design method for internal pavement crack recognition models using ground penetrating radar

Xin Yu [a,b,*], Chen Dong [a], Can Li [a], Di Li [b], Chen Chen [a,*], Haoran Zhu [a], Yangming Gao [c,**]

[a] College of Civil and Transportation Engineering, Hohai University, Nanjing, China
[b] College of Transportation Engineering, Changsha University of Science and Technology, Changsha, China
[c] School of Civil Engineering and Built Environment, Liverpool John Moores University, Liverpool, United Kingdom

ARTICLE INFO

Keywords:
Internal Pavement Cracks
3D Ground Penetrating Radar
YOLO Algorithm
Lightweight Model Design
Automated Crack Detection

ABSTRACT

Transverse cracks are among the most prevalent forms of damage in Semi-rigid asphalt pavements, traditionally the crack identified through manual methods that are time-consuming and suffer from poor consistency. To improve the efficiency of crack disease identification, this study employs a self-developed high-speed and high-precision 3D ground-penetrating radar to characterize internal crack defects. The You Only Look Once-v8n algorithm is enhanced through lightweight design, optimizing its backbone network and loss function while incorporating an attention mechanism to strengthen crack feature extraction, detection accuracy, and training stability. Practical engineering evaluations demonstrate that the algorithm reduces manual identification time by 50%, with over 60% of results achieving high expert validation rates. The missed detection counts for visible cracks are comparable to manual methods. This algorithm enables automated identification of internal cracks in pavement rehabilitation projects.

1. Introduction

Chinese highway infrastructure has expanded rapidly, presenting escalating maintenance challenges. By the end of 2024, Chinese total operational highway mileage has exceeded 5.49 million kilometers, including 190,000 km of expressways. Among the commonly used pavement structures, semi-rigid base asphalt pavements are widely applied due to their favorable mechanical performance and cost-effectiveness. However, the semi-rigid base layer is prone to transverse cracking due to material shrinkage (drying and thermal effects) coupled with vehicle loading. These cracks progressively propagate upward through the surface layer, forming reflective cracking. According to statistics from the latest national highway inspection statistics, transverse cracking is the most prevalent distress type in asphalt expressways across China. For instance, in Jiangsu Province, transverse cracks account for 88% of pavement distresses, with over 70% classified as internal cracks. Notably, crack quantities exhibit an annual upward trend, as illustrated in Fig. 1. In light of this, there is growing interest in the efficient detection and assessment of subsurface and reflective pavement cracks.

Conventional detection of internal cracks often relies on the core drilling method, which provides straightforward visual inspection but causes pavement damage and suffers from poor repeatability and representativeness. Ultrasonic testing, one of the widely adopted methods of nondestructive detection, has also been investigated for internal pavement defect assessment (Franesqui et al., 2017; Zhang et al., 2019; Tavassoti et al., 2022). Whereas, its practical applications are limited by low operational efficiency, significant measurement errors, and limited reliability. Ground-penetrating radar (GPR) has emerged as the preferred method for detecting cracks in pavement structures due to its high-resolution imaging capabilities, operational efficiency, continuous data acquisition, non-destructive operation, and real-time data acquisition. (Diamanti & Redman, 2012) numerically simulated the effects of crack filler materials, aperture width, vertical propagation depth, asphalt layer conductivity, and GPR center frequency on electromagnetic signature responses, demonstrating the feasibility of GPR in detecting and characterizing vertical cracks. (Krysinski & Sudyka, 2013) conducted laboratory-controlled GPR investigations on idealized crack prototypes to identify common radar signature patterns across different crack types, enabling depth estimation through electromagnetic waveform analysis. Their exploration of 3D imaging GPR diagnostic capabilities, using horizontal slicing visualization techniques, revealed

* Corresponding author at: Hohai University, No.1 Xikang Road, Nanjing, 210098.
** Corresponding author at: Liverpool John Moores University, Byrom Street, Liverpool, L3 3AF.
E-mail addresses: 20090002@hhu.edu.cn (X. Yu), 20230926@hhu.edu.cn (C. Chen), y.gao@ljmu.ac.uk (Y. Gao).

https://doi.org/10.1016/j.cacaie.2026.100028
Received 18 July 2025; Accepted 15 February 2026
Available online 6 April 2026

significant attenuation of crack signatures under low-contrast subsurface conditions. (Rasol et al., 2020) proposed a GPR-based method for identifying cracks in cement concrete through finite-difference time--domain (FDTD) numerical simulations, validating its potential in detecting cracks across diverse materials. (Fernandes & Pais, 2017) conducted GPR inspections on cracked asphalt concrete slabs, showing that crack detectability primarily depends on the contrast between surrounding layers and crack width. (Levatti et al., 2017) employed GPR to monitor cracks formed in soil samples during drying processes, revealing its capability to detect cracks as narrow as 1–2 mm, thereby confirming its potential for soil crack detection. (Torbaghan et al., 2020) improved image processing performance by integrating singular value decomposition (SVD) algorithms with median filters, successfully identifying cracks as narrow as 1.3 mm, thus validating applicability of GPR for automated pavement crack detection. (Fan et al., 2024) analyzed the impact of non-uniform interference on GPR-based crack identification in surface layers, finding that higher wave frequencies, wider crack apertures, and increased moisture content in cracks mitigate interference. Their study also established a mapping relationship between crack width and uniform reflected waveforms, emphasizing that filtering heterogeneous interference is prerequisite for detecting millimeter-scale cracks. (Zhu et al., 2025) utilized 3D GPR for pavement crack detection, identifying horizontal cross-sections as the primary diagnostic tool. Additionally, they proposed eight time-frequency domain electromagnetic signal features to enhance crack recognition, achieving over 95% identification accuracy.

With the continuous advancement of artificial intelligence technology, scholars have attempted to use AI algorithms to extract features of crack defects, achieving good results in automatic crack identification(Li et al., 2023; Lin et al., 2023; Malek et al., 2023; Chu et al., 2024). However, these technologies are mainly applied to the identification of surface cracks. The identification of internal cracks within pavements using ground-penetrating radar still relies on manual methods, which suffer from low efficiency and significant discrepancies in judgment results. Du and Liu systematically reviewed the current state of GPR detection technologies and characteristic signatures of internal distresses, critically evaluating the strengths and limitations of mainstream image processing techniques in identifying subsurface pavement defects, while pinpointing critical implementation challenges in practical engineering applications (Du et al., 2021; Liu et al., 2025) . (Liang et al., 2022) developed VGG16 and ResNet50 models based on deep convolutional neural networks (CNNs) for automated identification of typical internal pavement distresses. The results demonstrated that the VGG16 architecture achieved peak performance metrics of 98.73% accuracy, 97.98% precision, and 96.17% recall. (Xu et al., 2023) addressed the challenges of limited sample size and imbalanced data distribution in radar datasets by employing the Wasserstein Generative Adversarial Networks with Gradient Penalty (WGAN-GP) for data augmentation, achieving 90.85% classification accuracy through a ResNet50-based automated distress categorization model. Cha implemented convolutional neural networks (CNNs) for subsurface crack detection, achieving 97% recognition accuracy on asphalt pavements and 87.7% on concrete cracks. The algorithm demonstrated robust adaptability across varying acquisition conditions, fulfilling practical engineering requirements (Cha et al., 2017; Cha et al., 2018). Tong pioneered the application of convolutional neural networks (CNNs) to identify latent cracks in GPR images. Their methodology not only enables accurate crack localization but also extracts precise morphological features of cracks, significantly enhancing GPR image interpretation capabilities. Notably, Tong observed a progressive decline in CNN recognition accuracy with reduced GPR transmission frequencies, revealing a critical technical challenge for low-frequency subsurface crack detection systems (Tong et al., 2017; Tong et al., 2018). (Lahnsteiner et al., 2024) developed a synthetic data-driven automatic target detection method for multi-antenna GPR images, implementing a You Only Look Once (YOLO)-based framework to establish an end-to-end automated workflow encompassing data generation, processing, training, and application. (Chun et al., 2023) proposed an automated dataset annotation framework that integrates YOLOv5 with Style GAN2-ADA, employing generative adversarial networks for image synthesis. This methodology not only augmented the dataset scale but also demonstrated significant improvements in recognition accuracy. (Bae et al., 2025) conducted a comparative analysis of Mask R-CNN and YOLOv8 models for tunnel lining identification. The results indicate that while Mask R-CNN achieves higher recognition accuracy and precision, YOLOv8 demonstrates significantly faster processing speeds in both training and inference phases. (Li et al., 2022) developed a specialized pseudo-color mapping technique through systematic analysis of radar data preprocessing methods. By transforming reflected signals and incorporating radar reflection simulation for model pre-training, this approach achieved 72.39% recognition accuracy for shallow cracks.

The YOLO algorithm, as an end-to-end object detection framework, delivers significant advantages in processing real-time data due to its efficient inference speed and high detection accuracy. As such, YOLO has emerged as a critical technological solution for automated detection tasks, garnering substantial scholarly attention. (Bugarinović et al., 2024) generated 2000 synthetic radar images using the open-source electromagnetic simulation software gprMax. Training experiments demonstrated the effectiveness of the YOLO algorithm in automated GPR image interpretation, particularly exhibiting robust performance in analyzing hyperbolic reflection patterns characteristic of internal cracks. To enhance crack recognition accuracy, To tackle the issues of limited data availability and suboptimal data quality in GPR-based crack defect detection, (Liu et al., 2022) proposed a “Deep Augment” data augmentation strategy integrated with object detection models. This method significantly enhances the recognition accuracy and confidence scores for subsurface crack identification, with particularly pronounced improvements observed in YOLOv3 implementations. Hou and Chen

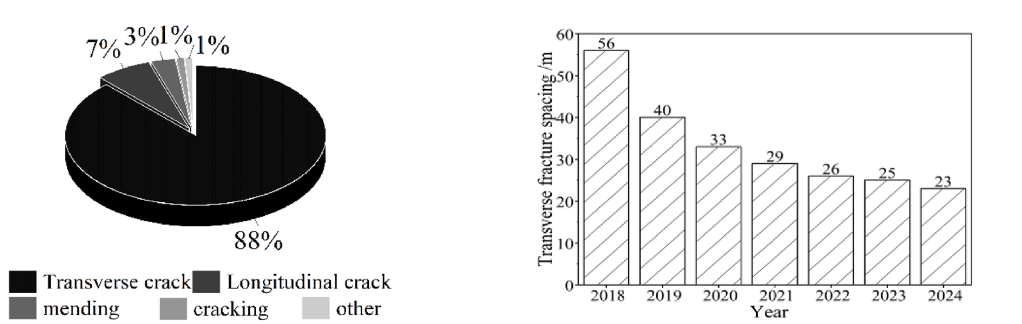

(a) Spatial Distribution of Pavement Distress on Jiangsu Expressways **(b) Development Trend of Transverse Cracks on a Selected Jiangsu Expressway**

Fig. 1. Distribution and development trends of crack distress in jiangsu province.

incorporated the RevCol module to replace the backbone networks of different YOLO models. Their results demonstrated consistent improvements across multiple metrics—including mAP@50, precision, and recall—with a notable 3.3% increase in recognition accuracy. Moreover, the model parameters and model size were reduced by over 50%(Chen et al., 2025; Hou et al., 2025). Arthur, Niu, and Wen demonstrated that integrating the CBAM attention module into the YOLO architecture effectively enhances the model's feature extraction capability and consistently improves detection accuracy(Niu & Yin, 2023; Arthur et al., 2024; Wen et al., 2024). (Liu et al., 2023) proposed an enhanced YOLOv3 model that integrates radar profiles with slice maps, incorporating a Four-Detection-Layer (FDL) architecture. This model enhances detection performance through multi-scale feature fusion, integrating the Efficient Intersection over Union (EIOU), K-means++ clustering, and hyperparameter optimization mechanisms to boost detection performance. Experimental results demonstrate that F1-score and the mean average precision (mAP) values of the model is 88.1% and 87.8%, respectively, establishing a robust foundation for three-dimensional characterization of pavement crack distresses. Xiong implemented the YOLOv4 algorithm on ground-penetrating radar (GPR) B-scan data for automated crack detection, achieving over 95% detection accuracy on test sets. Furthermore, a three-stage methodology was developed for automatic detection and localization of internal damage echo signatures in GPR images. This approach attained 96.99% comprehensive detection accuracy, with semantic segmentation precision exceeding 0.856 for damage-related pixels and a mean depth estimation deviation of 3.25 cm(Xiong et al., 2023; Xiong et al., 2024). (Zhang et al., 2023) investigated GPR image characteristics of subsurface concealed cracks with varying lengths and widths using the gprMax, and employed YOLOv5 to estimate crack vertical dimensions with a minimum error of approximately 1.3%. (Guo & Wang, 2023) implemented the YOLOv5 algorithm for automated identification of internal pavement distresses based on GPR-acquired data, achieving 88.2% recognition accuracy. (Huang et al., 2025) developed a grid-based processing framework utilizing the ECA-ResNet network to analyze GPR-acquired crack images. By detecting crack grid centroids as feature points and reconstructing continuous crack paths through tensor voting algorithms, this method achieved a 90% crack extraction rate, outperforming conventional object detection networks such as YOLOv5 and Fast R-CNN. (Liu et al., 2024) enhanced the YOLOv8 algorithm by incorporating a 160 × 160 output layer, integrating Selective Kernel Networks (SKNet) attention mechanisms, and adopting a Power Intersection over Union (IoU) loss function. These optimizations improved mAP and F1-score for crack detection by 6.3% and 5.9%, respectively. Additionally, the implementation of an unsupervised Auto-Augment strategy for crack dataset augmentation further boosted the enhanced mAP and F1-score of the model by 4.1% and 4.6%.

Despite extensive academic research on automated crack detection technologies, their practical implementation in engineering remains limited. This discrepancy primarily stems from three critical challenges: (1) Current crack detection algorithms often suffer from over-parameterization and high computational costs, which limit their scalability and efficiency; (2) The small size of cracks relative to radar wavelengths makes it difficult to accurately detect cracks, leading to significant identification errors when using hyperbolic signatures in B-scan images; (3) GPR measurements often produce false positives, where crack-like features appear in subsurface data due to noise or signal interference, necessitating robust false-positive filtration mechanisms.

To address the challenges of slow computational efficiency and insufficient crack feature extraction in current subsurface crack detection technologies, this study proposes an automated identification method based on a lightweight YOLO algorithm. The approach optimizes the YOLO backbone network and loss function while incorporating attention mechanisms. Crack defects are classified according to their expert validation frequencies within the dataset to enhance feature extraction capabilities. Additionally, leveraging GPR detection characteristics of internal cracks, a fusion frame coefficient R is introduced to filter out false positives with low fusion counts, thereby improving identification accuracy.

The remainder of this paper is organized as follows:

- Section 2 introduces the operational principles of 3D GPR and characterizes the electromagnetic signatures of internal cracks, with experimental validation.
- Section 3 details the computational hardware environment, protocols for crack dataset preparation, and distress classification methodology.
- Section 4 presents the lightweight algorithm architecture and the proposed crack detection framework, emphasizing model optimization strategies.
- Section 5 provides a comparative analysis of detection performance through quantitative benchmarking.
- Section 6 concludes the study with key findings and future research directions.

2. Subsurface crack damage detection theory

2.1. Detection mechanisms and data processing of 3D ground-penetrating radar

GPR operates by transmitting high-frequency electromagnetic waves (with center frequencies ranging from tens of megahertz to hundreds of megahertz and even up to gigahertz) as wideband short-pulse signals into the subsurface through a ground-based transmitting antenna T. When propagating through subsurface media, electromagnetic waves undergo reflection at locations where the dielectric permittivity differs from that of surrounding subsurface interfaces, ultimately returning to the surface for acquisition by the ground-mounted receiver antenna R. The system then performs imaging analysis of the received wavefield to reconstruct subsurface structural profiles, as illustrated in Fig. 2. Internal cracks, typically filled with air or free water, create localized dielectric constant variations that induce electromagnetic wave reflections, enabling non-destructive detection of subsurface cracking.

However, electromagnetic waves experience progressive energy attenuation during propagation, resulting in weak received signals contaminated by interference such as system noise, ambient noise, and subsurface anomalies. These distortions degrade imaging quality, necessitating advanced preprocessing to suppress noise artifacts and enhance crack signatures prior to data interpretation. Fig. 3 illustrates the standard preprocessing workflows and their implementation sequences.

2.2. Radar signature characteristics of crack distresses and validation

Internal cracks, as the predominant distress type in semi-rigid base asphalt pavements, typically beginning as internal fractures within the

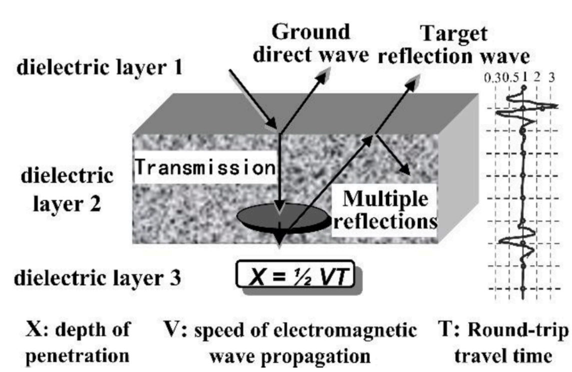

Fig. 2. Operational principle of GPR detection.

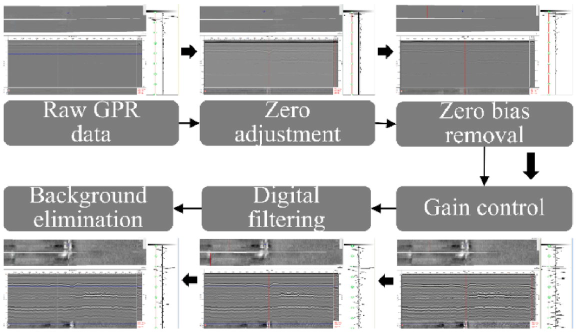

Fig. 3. Preprocessing workflows and effects of GPR data.

base layer. These fractures gradually propagate and expand, eventually penetrating the surface layer. This study employed a high-speed, high-resolution 3D GPR system independently developed by the research team to detect internal cracks, with validation through field coring. The results demonstrate that the system can precisely identify millimeter-scale internal cracks within pavement structures, as illustrated in Fig. 4.

When GPR electromagnetic waves encounter internal cracks, scattering occurs due to the small dimensions of the cracks and dielectric inhomogeneity caused by air/water-filled voids. Scattered waves undergo reflection at pavement structural interfaces, yet only those from interfaces proximal to cracks are effectively captured by the closely spaced transceiver antennas. Furthermore, in semi-rigid base layers where cracks typically propagate through entire structural layers, internal cracks manifest as linear anomalies in radar slices adjacent to interfaces. These anomalies exhibit distinct “blur-clear-blur” amplitude variations along their propagation paths, as demonstrated in Fig. 5.

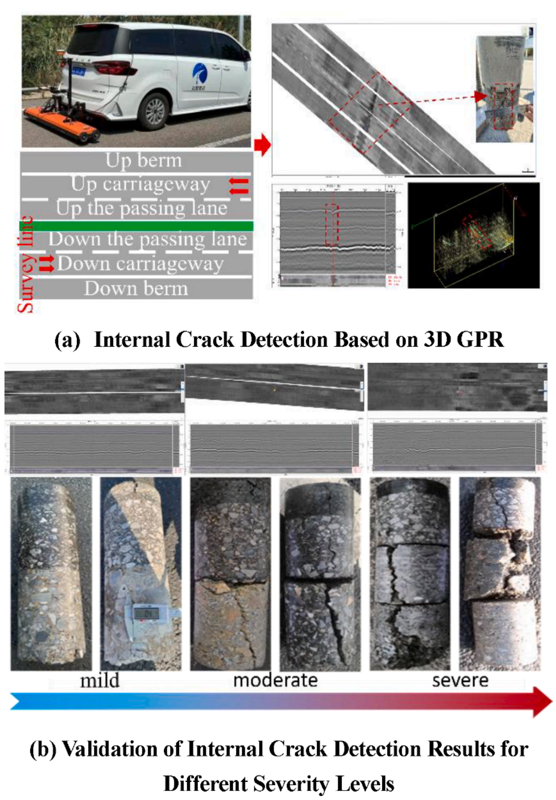

Fig. 4. 3D GPR imaging and core validation of internal cracks.

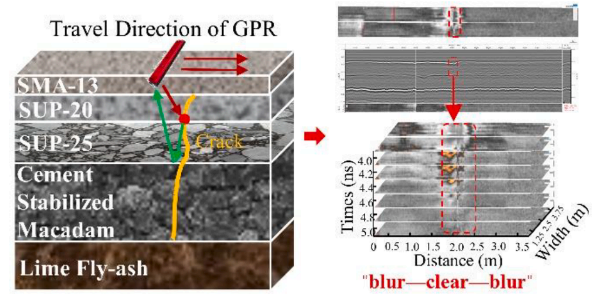

Fig. 5. Signature characteristics of subsurface crack distresses in GPR imagery.

3. computational environment and dataset

3.1. Hardware configuration and computational environment

This study utilized a high-performance computer for model computation, with a hardware configuration consisting of a 64-bit Windows 11 operating system. The central processing unit (CPU) used was an Intel® Core™ i9–13900 K, and the graphics processing unit (GPU) was an NVIDIA RTX 4090. The system was equipped with 32 GB of main memory and 24 GB of video memory. The programming language employed was Python 3.11, and model training was conducted using the deep learning framework PyTorch 2.1.2, leveraging the GPU acceleration capabilities of CUDA 11.8 and CUDNN 8.7.

To further enhance the efficiency and stability of the training process, the project adopted an appropriate input image size of 640 × 640 pixels and set the batch size to 32. This configuration ensured sufficient data processing per training iteration while maintaining reasonable memory usage. The Adam W optimizer was selected, combined with a learning rate of 0.001 and a momentum of 0.937, which effectively accelerated model convergence and mitigated gradient-related issues

3.2. Crack distress dataset development

This study comprehensively considered factors such as geographical location, traffic load, and pavement age to select crack disease detection and on-site core sampling results from 11 typical highway sections in Jiangsu Province. A total of 1687 crack disease datasets were compiled. Since crack diseases exhibit more distinct characteristics in radar slice images, and due to the relatively sparse distribution of detection points in the vertical formation direction, directly resizing images to 640 × 640 would cause distortion of crack features. Therefore, this study generated 640 × 174 pixel pavement internal crack images through image padding techniques. Furthermore, as discussed in Chapter 2, crack disease characteristics demonstrate a "blur-clear-blur" pattern along the depth direction, with variations observed across different severity levels. Accordingly, this study defines severe crack slices (3 slices) near layer interfaces as Confirmed Cracks CA, and all other cracks as Suspected Cracks CB. The characteristic patterns of CA and CB crack diseases are illustrated in Fig. 6.

4. Proposed method

4.1. You only look once-v8 model architecture selection

The YOLO framework adopts an end-to-end approach by formulating object detection as a regression task, simplifying traditional detection workflows while significantly improving processing speed. As the lightweight variant of the YOLOv8 series, YOLOv8n retains the feature extraction capabilities, detection accuracy, and speed of its predecessor. At the same time, it drastically reducing computational costs through a simplified backbone network, streamlined feature fusion layers, and

(a) Representative Examples of CA

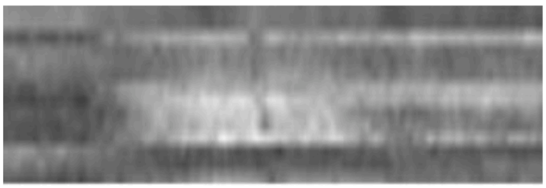

(b) Representative Examples of CB

Fig. 6. Dataset categorization with CA and CB samples.

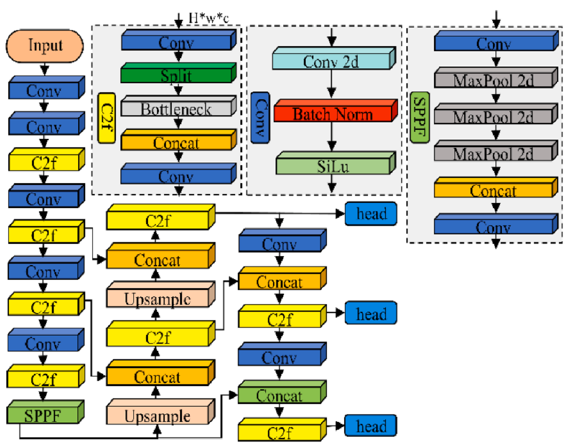

Fig. 7. Architectural schematic of the YOLOv8n network.

optimized detection head design. Fig. 7 illustrates the architectural schematic of YOLOv8n.

4.2. Optimization of you only look once-v8n algorithm for the detection of subsurface crack

The YOLOv8n model performs well in conventional object detection tasks. However, it exhibits limitations when addressing challenges such as significant scale variations and complex backgrounds, which are common in detecting internal cracks. To overcome these limitations, this study enhances the YOLOv8n algorithm to better capture the elongated morphology, complex shapes, irregular boundaries, and noise-sensitive characteristics of cracks in radar images. The improvements include three key modifications: first, replacing the original backbone network with a Reversible Convolutional Network (RevCol) to preserve low-level texture details and minimize information loss for thin, intricate cracks; second, integrating a Convolutional Block Attention Module (CBAM) to focus on crack regions while suppressing background noise; and third, adopting an EIOU to improve bounding box localization accuracy. These optimizations collectively enhance crack feature extraction and detection precision.

(1) Optimized backbone network for lightweight performance

In object detection tasks, the choice of the backbone network directly impacts the model's feature extraction capability. The traditional YOLOv8n model employs a combination of CSP and SPPF modules to efficiently extract image features at minimal computational cost. However, this network architecture operates as a feedforward structure where each layer's input depends solely on the output of the preceding layer, making it challenging to accurately capture fine-grained features such as cracks.

The RevCol network operates through its core reversible convolutional layers. Input images are first divided into smaller blocks, which are then processed independently using reversible convolutions. This design mitigates information loss inherent in traditional convolutional operations by preserving gradient flow across layers, as mathematically formulated in Eq. (1).

$$X_l = F_l(X_{l-1}) + X_{l-1} \tag{1}$$

In the equation, $X_l$represents the feature map of the L-th layer; F_l denotes the convolution operation of this layer; X_{l-1} is the input feature map from the $(l-1)$-th layer.

The RevCol network employs multi-layer reversible convolution blocks to fuse features extracted at each hierarchical level, maintaining unimpeded information flow through residual connections. This architectural design effectively mitigates the gradient vanishing problem, which is common in traditional convolutional neural networks. It also processes multi-scale target information efficiently, thereby enhancing robustness in crack detection. Fig. 8 illustrates the RevCol network architecture, highlighting its core components: individual reversible convolution blocks, reversible fusion blocks, and the comprehensive reversible columnar network structure.

(2) Attention mechanism integrated

Due to the multiple interlayer reflections of electromagnetic waves during subsurface propagation, the returned echo signals can introduce noise interference in slice images, significantly impairing the model's ability to extract crack disease features. To more effectively capture these features, this study incorporates the Convolutional Block Attention Module (CBAM) into the YOLOv8n architecture. This module consists of both channel attention and spatial attention components, which work to amplify feature responses in minute regions containing small targets while suppressing those in background areas, thereby effectively mitigating interference from complex backgrounds.

The channel attention mechanism generates attention maps by sequentially applying global average pooling and global maximum pooling to input feature map F. These pooled features are then processed through fully connected (FC) layers to generate channel-wise attention weights, which are multiplied with F to emphasize crack-sensitive frequency components. This operation is mathematically expressed as Eq. (2):

$$\begin{gathered} M_c(F)= \sigma(FC(ReLU(FC(GAP(F)))) + FC(ReLU(FC(GMP(F))))) \\ F' = F \cdot M_c(F) \end{gathered} \tag{2}$$

The Spatial Attention Mechanism processes the feature map obtained from the Channel Attention Mechanism by applying Max Pooling and Average Pooling along the channel dimension. These pooled feature maps are then concatenated channel-wise to generate a spatial attention map, which highlights regions containing crack morphology. This operation is formulated as Eq. (3):

$$M_s(F') = \sigma(Conv([MaxPool(F'); AvgPool(F')])) \tag{3}$$

In the equation, σ is the activation function of sigmoid, *σ_x=x/(1 + e^ (-x)); FC(•)* denotes the fully connected layer;*[;]* denotes concatenation along the channel dimension.

The CBAM structure is illustrated in Fig. 9.

(3) Loss Function Modification

Although crack diseases appear as elongated, strip-like features in slice images, their varying developmental directions significantly

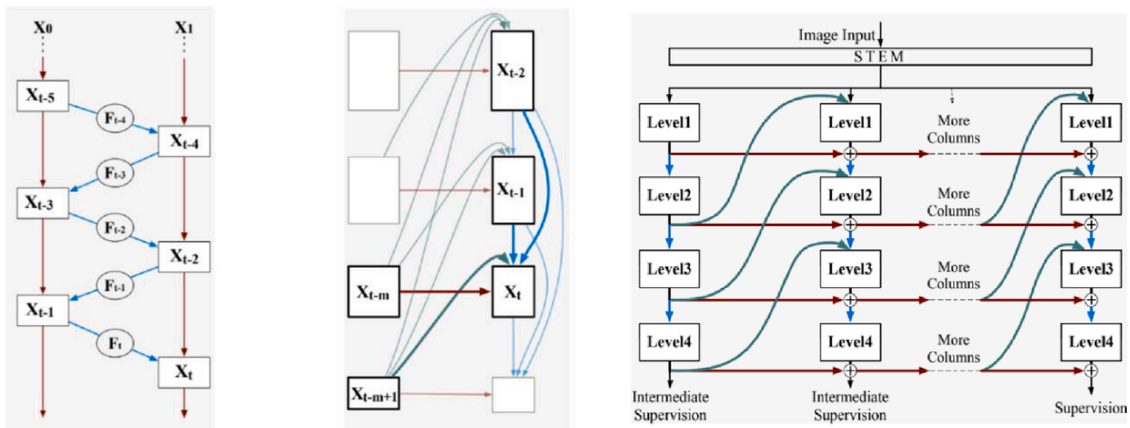

（a） **Reversible convolution blocks** （b） **Reversible fusion blocks** （c） **Reversible columnar network architecture**

Fig. 8. Architectural schematic of the RevCol network.

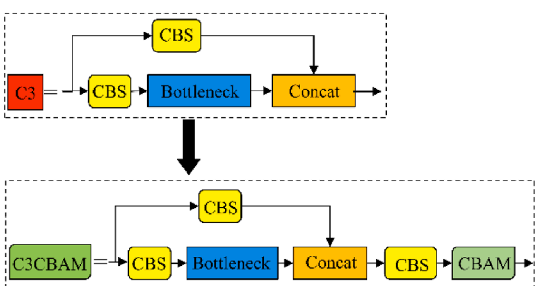

Fig. 9. Architectural schematic of the CBAM attention mechanism.

impact the aspect ratio of model-predicted bounding boxes. The CIOU loss function in YOLOv8 is overly sensitive to aspect ratio variations, which can lead to localization inaccuracies when dealing with irregularly shaped, multi-scale small targets. This impairs bounding box regression precision and results in poor model robustness in complex backgrounds. To address this limitation, this paper introduces a modified loss function by incorporating the EIOU loss. This approach comprehensively evaluates both bounding box shape and relative positioning, thereby optimizing the regression process. By reducing CIOU's excessive reliance on aspect ratios in complex scenarios, the enhanced loss function enables more precise detection of fine cracks and similar targets. Fig. 10 illustrates the computational workflows of the two loss functions.

The EIOU loss function can be formulated as Eq. (4):

$$L_{EIOU} = 1 - \frac{|A \cap B|}{|A \cup B|} + \lambda \cdot d(b, b') \tag{4}$$

In the equation, L_{EIOU} denote the EIOU loss; $|A \cap B|$and$|A \cup B|$represent the intersection and union areas between the predicted bounding box and the ground-truth box respectively;$\lambda$is a weighting coefficient;$d(b, b')$ uantifies the shape discrepancy between boxes;b, b'correspond to the positional coordinates and dimensional parameters of the predicted and ground-truth boxes.

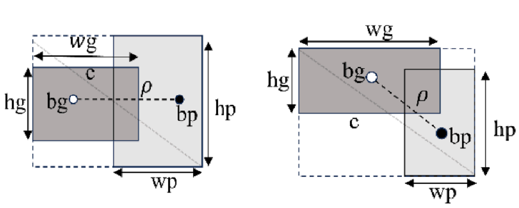

（a）**CIOU** （b）**EIOU**

Fig. 10. Computational comparison of loss functions.

4.3. Crack distress identification based on 3D ground-penetrating radar

To facilitate practical engineering application of the automated pavement crack detection methodology, this study processes GPR slice data by composing each slice from 320-trace electromagnetic wave data to generate crack distress detection inputs. The algorithm-derived bounding boxes are then converted into corresponding GPR trace numbers using Eq. (5), enabling seamless integration of detection results with original radar acquisition coordinates.

$$\begin{aligned} n_1 &= N + 320 \ \times (x - w/2) \\ n_2 &= N + 320 \ \times (x + w/2) \end{aligned} \tag{5}$$

Here, *n1*和*n2* denote the left and right trace numbers of the bounding box, respectively; N represents the minimum trace number within the GPR slice image containing the crack distress; The parameter x corresponds to the normalized coordinate of the bounding box center, scaled to the range [0,1]; while w indicates the normalized width of the bounding box within the same range.

Furthermore, recognizing the inherent depth-wise continuity of crack distresses within pavement structures, this study introduces the Fusion Frame Count Index R to refine detection accuracy. This metric operates by analyzing the spatial distribution of detected cracks: bounding boxes with overlapping regions are merged as representing a single continuous crack, while isolated detections lacking overlap with adjacent boxes are filtered as spurious features. Through this consolidation mechanism, the algorithm effectively suppresses false positives caused by fragmented or noise-induced detections, thereby enhancing overall recognition precision.

5. Results and discussion

5.1. Performance comparison and analysis of model enhancements

(1) Evaluation Metrics

To evaluate the performance of the proposed model in road crack detection, this study employs precision (P), recall (R), mean average precision (mAP), giga floating-point operations (GFLOPs), and parameter count (Params) as evaluation metrics. Precision is defined as the ratio of correctly predicted positive crack samples to all samples predicted as positive by the model. Recall represents the proportion of actual positive crack samples that are correctly identified. The F1-score serves as a comprehensive metric that harmonizes precision and recall, calculated as the harmonic mean of these two values. The mAP metric captures the dynamic relationship between precision and recall across different thresholds, with mAP@50 specifically denoting the mean average precision at an Intersection over Union (IoU) threshold of 0.5.

$$P = \frac{T_p}{T_p + F_p} \tag{6}$$

$$R = \frac{T_p}{T_p + F_N} \tag{7}$$

$$F_1 = \frac{2 \times P \times R}{P + R} \tag{8}$$

$$A_p = \int_0^1 P(R)dR \tag{9}$$

$$mAP = \frac{1}{n}\sum_{i=0}^{n} A_{p_i} \tag{10}$$

In the equations, *Tp* represents the number of correctly identified crack instances; *Fp* denotes the number of non-crack instances erroneously classified as cracks; F_N indicates the number of crack instances incorrectly predicted as non-cracks; *P(R)* represents the precision-recall curve with *R* as the horizontal axis and *P* as the vertical axis; n denotes the number of categories, set to 2 in this experiment; and AP_i refers to the average precision for the i th category.

Furthermore, to assess the model's computational capacity and inference speed, both the number of parameters (Params) and computational complexity (GFLOPs) are adopted as evaluation metrics. It should be noted that a higher GFLOPs value indicates greater computational capability.

(2) Data augmentation and Dataset Categorization

To enhance the generalization capability of the identification model, mitigate overfitting, and improve its adaptability and robustness in complex environments, this study performed data augmentation on the established dataset. The augmentation techniques included: (1) geometric transformations such as flipping, rotation, and cropping; (2) color transformations including brightness adjustment, contrast enhancement, saturation modification, and sharpening; (3) random occlusion; and (4) noise addition. The augmented dataset was then randomly divided into training, validation, and test sets in an 8:1:1 ratio. The differences in identification performance before and after data augmentation and dataset categorization are detailed in the Table 1. As evidenced by the table, following the division of crack defects in the dataset into CA and CB categories, while the identification accuracy experienced a slight decline, the recall rate demonstrated a notable improvement—increasing by approximately 6%—with the mAP@50 metric also rising by 5%. Building upon this foundation, the implementation of data augmentation techniques further enhanced the recall rate for crack identification results by an additional 5.5%, accompanied by a 2% increase in mAP@50.

Table 1
Comparison of identification performance before and after data augmentation.

		P	R	mAP@50	F1 Score
categorized Data	Before Augmentation	83.8	76.2	76.2	80.1
	After Augmentation	83.7	80.4	77.7	82.0
Non-categorized Data	Before Augmentation	84.1	72.2	72.9	78.3
	After Augmentation	84.4	75.5	73.5	80.6

(3) Training Process Analysis

This study compares the mAP@0.5 and Total_Loss between the baseline and optimized networks to investigate the impact of integrated component configurations on the network, as shown in Fig. 11. Fig. 11 reveal that the enhanced network achieves faster convergence after 350 epochs of training, attaining the optimal mAP@0.5 value. Furthermore, the enhanced network consistently outperforms the original YOLOv8n in mAP@0.5 throughout the training process, with a significant reduction in Total_Loss. These results demonstrate that the proposed enhancements substantially improve detection accuracy and training stability, validating the effectiveness of the optimized model.

(4) Ablation Study

To validate the performance improvements of the modified YOLOv8n network over the original model and assess the contributions of individual enhancement components, this study conducts eight ablation experiments comparing the baseline network with progressively optimized versions. The comparative results are detailed in Table 2.

In the experimental study, Group A served as the baseline model. In Group B, after introducing the RevCol backbone network, precision improved to 82.5%, with recall reaching 71%, mAP@50 at 74.6%, Giga Floating-point Operations Per Second (GFLOPS) reduced to 6.3 G, and parameters decreased to 2.3 M. Group C, incorporating the CBAM attention mechanism, achieved further precision gains to 82.7%, recall of 73.2%, mAP@50 of 78.1%, while maintaining GFLOPS at 8.2 G and parameters at 3.0 M. Group D, utilizing the EIOU loss function, attained 81.8% precision, 74.3% recall, and 73.3% mAP@50, with GFLOPS and parameters unchanged. Group E, combining RevCol and CBAM, achieved 82.4% precision, 77.2% recall, and 77.1% mAP@50, retaining GFLOPS and parameter levels. Group F, integrating RevCol and EIOU, resulted in 81.8% precision, 77.5% recall, and 76.5% mAP@50, with GFLOPS reduced to 6.3 G and parameters to 2.3 M. Group G, employing CBAM and EIOU, achieved the highest precision of 83.5%, 74.6% recall, and 76.0% mAP@50, maintaining GFLOPS and parameters. Finally, Group H, combining RevCol, CBAM, and EIOU, delivered optimal performance with 83.7% precision, 80.4% recall, and 77.7% mAP@50, alongside reduced GFLOPS to 6.3 G and parameters to 2.3 M. These results demonstrate that individually introducing the RevCol backbone, CBAM attention, or EIOU loss effectively enhances model accuracy. Moreover, combining multiple blocks yields significant improvements in precision while maintaining computational efficiency, achieving an optimal balance between performance and resource utilization.

Furthermore, the Precision-Recall (P-R) curves of crack distress identification results before and after optimization are shown in Fig. 12. The figure demonstrates that the PR curve of the YOLOv8n algorithm incorporating RevCol, CBAM, and EIOU loss functions is closer to the (1,1) position and encompasses a larger area. This indicates enhanced feature extraction capabilities for both CA and CB crack distresses, resulting in more accurate and comprehensive detection outcomes.

(5) Comparation

To validate the advantages of the enhanced YOLOv8n in detecting internal cracks, this study conducts a comparative evaluation of multiple canonical YOLO-based object detection models on a subsurface crack defect dataset. Through comparative experiments, this work provides a detailed analysis of each performance of models across multiple evaluation metrics. The experimental results are summarized in Table 3.

In terms of precision (P), the enhanced YOLOv8n demonstrates

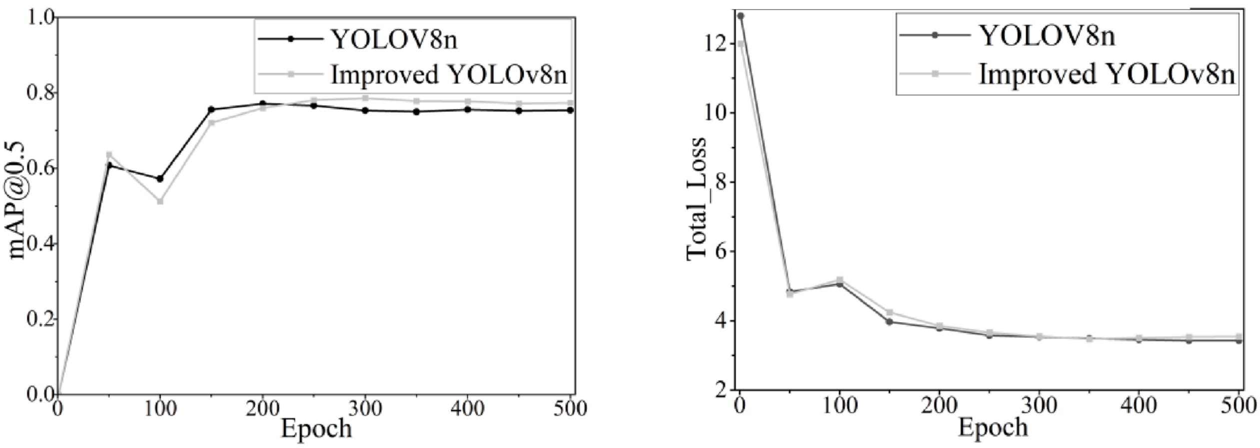

(a) comparison of mAP@0.5 (b) comparison of Total_Loss

Fig. 11. Training curve trends.

Table 2
Ablation study results.

Experi-ment ID	Rev-Col	CBAM	EIOU	P/%	R/%	mAP@50/%	GFLOPS/G	Parameters/M
A	∘	∘	∘	80.7	74.7	75.7	8.1	3.0
B	•	∘	∘	82.5	71	74.6	6.3	2.3
C	∘	•	∘	82.7	73.2	78.1	8.2	3.0
D	∘	∘	•	81.8	74.3	73.3	8.2	3.0
E	•	•	∘	82.4	77.2	77.1	8.2	3.0
F	•	∘	•	81.8	77.5	76.5	6.3	2.3
G	∘	•	•	83.5	74.6	76	8.2	3.0
H	•	•	•	83.7	80.4	77.7	6.3	2.3

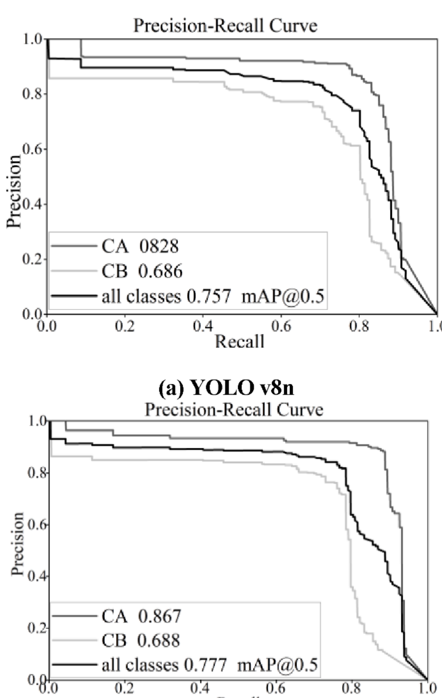

(a) YOLO v8n

(b) Improved YOLO v8n

Fig. 12. P-R curves before and after optimization.

Table 3
The result of comparation.

Models	P/%	R/%	mAP@50/%	F1 Score	GFLOPS/G	Parameters/M
YOLOv3	73.9	72.6	71.9	73.2	282.2	103.7
YOLOv3-tiny	77.8	70.2	71.6	73.8	18.9	12.1
YOLOv5n	78.1	80.6	77.2	79.3	7.1	2.5
YOLOv5s	78.0	74.1	76.5	76.0	23.8	9.1
YOLOv5m	79.3	77.8	77.2	78.5	64.0	25.0
YOLOv6n	78.6	79.1	77.0	78.8	11.8	4.2
YOLOv6s	77.0	77.8	75.3	77.4	44.0	16.2
YOLOv8s	80.9	79	77.2	79.9	28.4	11.1
YOLOv8n	80.7	74.7	75.7	77.6	8.9	3.3
YOLOv9s	78.7	77.8	74.7	78.2	26.7	7.2
YOLOv10n	78.3	68.9	67.2	73.3	6.5	2.3
YOLOv10s	79.3	76.1	75.1	77.7	21.4	7.2
YOLOv12n	81.2	74.2	76.0	77.8	9.2	3.5
Faster-RCNN	77.2	72.4	71.5	73.2	36.5	20.3
SSD	75.2	71.3	68.2	71.4	42.3	33.4
Improved YOLOv8n	83.7	80.4	77.7	82.0	6.3	2.3

superior performance, achieving 83.7% – significantly outperforming other models. Comparatively, YOLOv8s attains 80.9% precision, slightly lower than the enhanced version yet remaining competitive. Other models such as YOLOv5n and YOLOv3-tiny exhibit reduced precision at 78.1% and 77.8%, respectively. These results confirm the enhanced substantial advantage of YOLOv8n in recognition accuracy, making it particularly suitable for crack detection tasks requiring high precision.

In terms of recall (R), YOLOv5n achieves the highest performance at

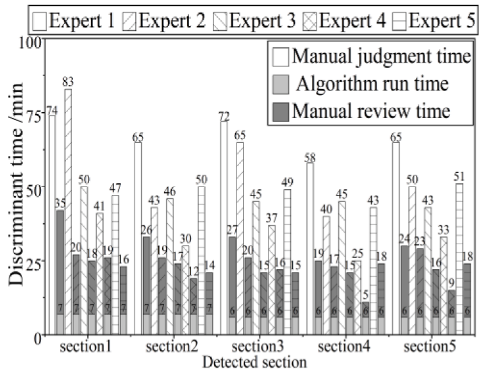

Fig. 13. Time comparison for subsurface crack identification.

80.6%, demonstrating its capability to detect a greater number of crack targets. The enhanced YOLOv8n closely matches this with a recall rate of 80.4%, maintaining strong detection proficiency. Other models, such as YOLOv3-tiny and YOLOv10n, exhibit lower recall rates at 70.2% and 68.9%, respectively. Since recall directly impacts the missed detection rate, higher recall values reduce oversight and improve the comprehensiveness of detection.

In terms of mAP@0.5, the enhanced YOLOv8n also demonstrates exceptional performance, achieving 77.7%, slightly surpassing 77.2% which demonstrated by YOLOv8s. Both YOLOv5n and YOLOv5m attain an mAP@0.5 of 77.2%, indicating their balanced performance in precision and recall, making them suitable for crack detection applications. In contrast, YOLOv10n achieves only 67.2% mAP@0.5, highlighting significant room for improvement in detection accuracy.

In terms of F1-score performance, the enhanced YOLOv8n achieves an F1-score of 82.0%, outperforming all other comparative models. Since the F1-score holistically balances precision and recall, this higher value demonstrates the enhanced exceptional comprehensive performance of YOLOv8n in crack detection tasks, effectively harmonizing accuracy and coverage.

In terms of computational complexity measured by GFLOPS, YOLOv3 exhibits the highest computational demand at 282.2 GFLOPS due to its substantial model complexity. In contrast, the enhanced YOLOv8n requires only 6.3 GFLOPS, enabling it to maintain high detection accuracy even in hardware-constrained environments. Other models, such as YOLOv3-tiny and YOLOv5n, demonstrate moderate computational requirements with 18.9 GFLOPS and 7.1 GFLOPS, respectively.

In the comparison of model parameters (M), the enhanced YOLOv8n exhibits a parameter count of 2.3 M. This reduced parameter count lowers its demands on storage and computational resources, making it advantageous for pavement crack detection tasks with high real-time requirements. In contrast, YOLOv3 has 103.7 M parameters. While its more complex architecture provides certain capabilities, this also results in significantly higher computational demands.

The results reveals that the enhanced YOLOv8n maintains consistently high F1-scores and mAP@0.5 values throughout the training process, indicating stable performance and superior detection accuracy compared to other models. When comprehensively evaluating all metrics, the enhanced YOLOv8n emerges as the optimal choice for subsurface crack detection. It achieves high detection precision while significantly reducing computational resource consumption and improving overall detection efficiency. Consequently, the enhanced YOLOv8n demonstrates the strongest potential in this study and holds broad application prospects for practical engineering deployments.

5.2. Evaluation of crack distress identification results in practical engineering applications

This study evaluates the enhanced YOLOv8n algorithm using five 1-km pavement sections from typical Jiangsu Province expressways. The frame fusion index R is calculated based on the quantity “n” of CA and CB crack defects identified by the YOLOv8n model at the same location.

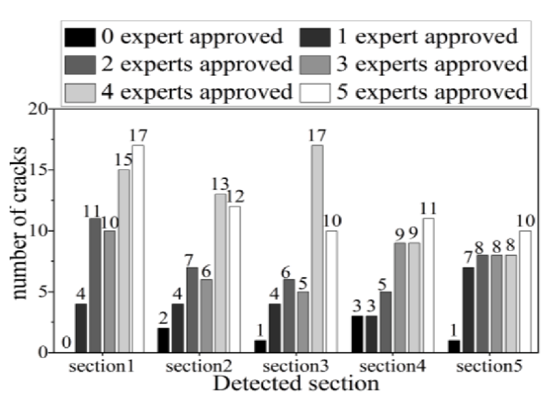

Fig. 14. Expert validation of auto-identification results.

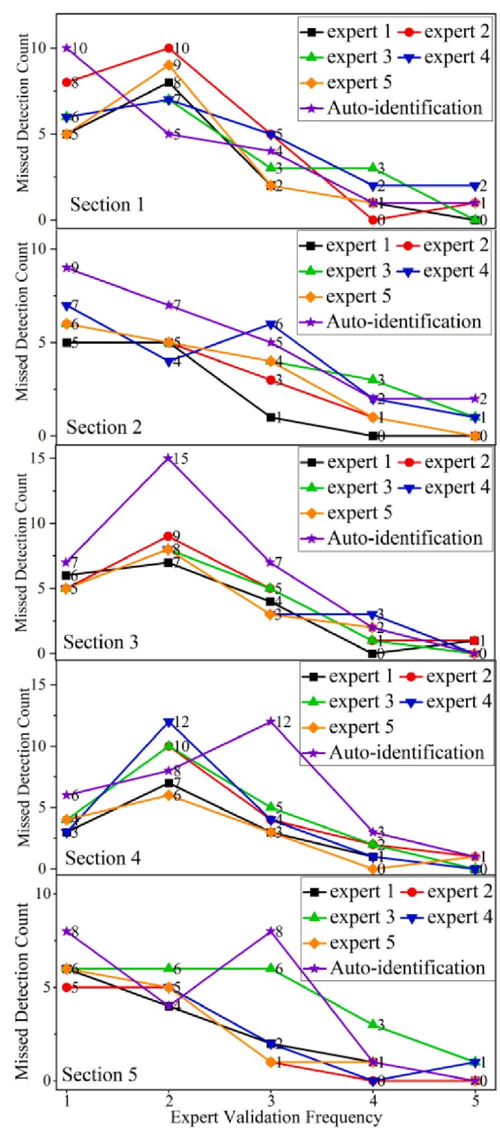

Fig. 15. Comparison of missed detections between manual and automated identification.

Identification results with an R value less than 2 are subsequently filtered out, thereby optimizing the automated detection outcomes. Here,

$$R = n - 1 \tag{11}$$

Furthermore, discrepancies between manual inspections and AI-based crack distress judgments are analyzed, assessing the effectiveness of automated detection across three dimensions: processing time, result acceptance rate, missed detection rate, and then 15 internal crack locations identified by the automated algorithm were randomly selected for on-site core sampling validation.

(1) Processing Time

The study sequentially recorded the time required for manual identification of defects, software-based identification, and manual verification of the results of software, as shown in Fig. 13. The data indicates that the software completes the identification process for 1 km of detection data within 6–7 min, while manual identification requires approximately one hour. Although the automatically identified results still require manual verification, the total time required is only about 50% of that needed for manual identification alone. This demonstrates that the automatic identification software developed in this study can effectively enhance the efficiency of crack defect identification.

(2) Validation of Identification Results

The identification algorithm employed in this study detected 50 crack defect data points per kilometer. An analysis of expert validation results for subsurface crack identification in five typical road sections is presented in Fig. 14. The data shows that over 90% of the automatically identified results received expert endorsement, with more than 60% of these results obtaining consensus approval from a majority of experts. Furthermore, the defect identification demonstrates relatively high accuracy.

(3) Analysis of Missed Crack Defect Identification

This study selects five typical road sections in Jiangsu Province for analysis. The manually validated automated detection results and manually annotated results were statistically analyzed, with their consolidated dataset serving as the ground truth data for defect verification across these sections. Missed detections from individual experts and the automated system, along with their corresponding expert validation frequencies, which was illustrated in Fig. 15.

The results show that the automated algorithm exhibited a marginally higher missed detection rate, approximately 1.2 times that of manual identification. However, these omissions predominantly involved defects with low expert validation frequencies. For defects demonstrating high validation consensus, no statistically significant difference in missed detection rates was observed between automated and manual methods.

(4) Validation of Identification Results

To enhance the reliability of the research findings, fifteen crack locations identified by the automated detection algorithm were randomly selected for on-site core validation. The coring results demonstrated that among the fifteen validated locations, only one site showed no crack presence, achieving a crack identification accuracy exceeding 90%. The characteristic patterns of typical internal crack defects and their corresponding core verification results are presented in Table 4.

Table 4
Automated identification results of internal crack defects and corresponding core verification.

Expert Validation Frequency	Internal Crack Defect Imagery	Core Validation Results
Frequency =4	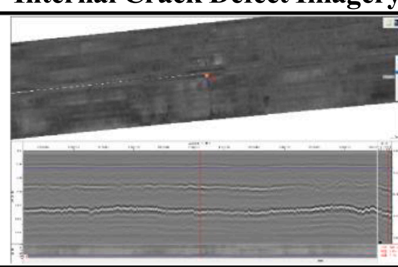	 
Frequency =3	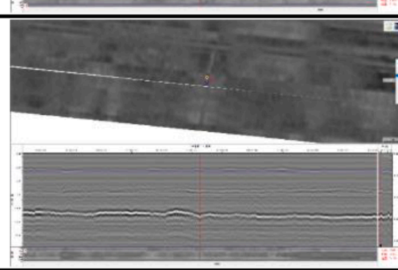	 
Frequency =2	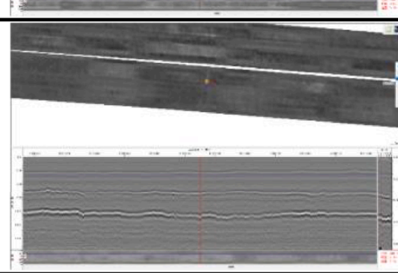	 

6. Conclusion

Current manual methods for identifying subsurface crack defects are limited by low efficiency and high result variability. To address these limitations, this study employed a self-developed 3D ground-penetrating radar with high speed and precision system analyze crack characteristics. Additionally, a lightweight YOLOv8n-based algorithm was designed to enhance crack feature extraction, with its performance benchmarked against manual identification in practical engineering applications. Within the scope of this research, the following conclusions can be drawn:

(1) To address the characteristics of crack diseases in radar images—such as their slender, complex morphology and irregular boundaries—this study enhanced the YOLOv8n algorithm by modifying its backbone network and loss function, supplemented with an attention mechanism, to improve detection performance. Experimental results show that the optimized model achieves mAP@50 and F1 scores of 77.7% and 82%, respectively. Compared to Faster-RCNN, SSD, YOLOv5n, YOLOv6n, YOLOv8n, YOLOv9s, YOLOv10s, and YOLOv12n, the proposed model improves mAP@50 by 8.7%, 13.9%, 0.65%, 0.9%, 2.6%, 4.0%, 3.5% and 2.2%, respectively, while F1-score improvements are 12%, 14.8%, 3.4%, 4.2%, 5.7%, 4.9%, 5.5% and 5.4%. These results demonstrate that the proposed model exhibits clear advantages in both mAP@50 and F1 score, with an overall significant improvement in detection performance.

(2) In terms of deployment efficiency, the proposed model has 2.3 M parameters and 6.3 G FLOPs, representing reductions of 30% and 29.2% compared to the YOLOv8n model. This enables rapid detection of internal pavement cracks. It is evident that the lightweight design of YOLOv8n in this study is achieved through structural innovation rather than simple pruning, thereby avoiding the loss of detection accuracy typically associated with conventional lightweight methods.

(3) Building upon the optimization of the YOLOv8n algorithm, this study proposes filtering detection results with fewer than 2 bounding box fusion occurrences and analyzes the crack detection outcomes in practical engineering contexts. The results indicate that the automatic recognition algorithm achieves high manual approval rates, with over 60% of the results recognized by more than half of the experts. The number of missed detections is slightly higher than that of manual inspection—approximately 1.2 times the manual miss rate—yet most of these missed cases correspond to results with low expert approval rates. For highly approved crack instances, the miss rate shows no significant difference from manual results. Moreover, the proposed method improves manual inspection efficiency by over 50%.

The crack disease recognition developed in this study focuses on internal crack data detected from highways in Jiangsu Province. In the future, the crack dataset can be iterated by incorporating detection results from other regions to further analyze and enhance the algorithm's recognition performance. While this study primarily focuses on optimizing the YOLO algorithm, future work could integrate classification algorithms, dynamic ensemble learning methods, and self-supervised learning approaches to further enhance the algorithmic model. Moreover, incorporating the automatic identification algorithm into road maintenance decision-support systems would significantly elevate the engineering application value of the research outcomes.

Funding information

National Key R&D Program of China, Grant/Award Number: SQ2024YFF0600120; National Natural Science Foundation of China, Grant/Award Number: 5237080727; Key R&D Program of Jiangsu, Grant/Award Number: JETC-DLJS-2024–005;

CRediT authorship contribution statement

Xin Yu: Writing – review & editing, Supervision. **Chen Dong:** Investigation, Conceptualization, Writing – original draft, Writing – review & editing. **Can Li:** Investigation, Methodology, Formal analysis, Writing – original draft. **Di Li:** Methodology, Writing – review & editing. **Chen Chen:** Investigation, Writing – review & editing. **Haoran Zhu:** Writing – review & editing. **Yangming Gao:** Investigation.

Declaration of competing interests

The authors declare that they have no known competing financial interests or personal relationships that could have appeared to influence the work reported in this paper.

Acknowledgments

This work was supported in part by the National Key R&D Program of China under Grant Number (SQ2024YFF0600120); National Natural Science Foundation of China (5237080727); Key R&D Program of Jiangsu (JETC-DLJS-2024–005).

References

Arthur, E., Aboah, A., & Huang, Y. (2024). A novel FHWA-compliant dataset for granular vehicle detection and classification. *IEEE access : Practical innovations, open solutions, 12*, 158505–158518.

Bae, B., Choi, Y., Jung, H., & Ahn, J. (2025). Tunnel lining segmentation from ground-penetrating radar images using advanced single- and two-stage object detection and segmentation models. *Computer-Aided Civil and Infrastructure Engineering, 40*(22), 3580–3592.

Bugarinović, Ž., Gavrilović, M., Ristić, A., Bugarinović, M.Š., Radulović, A., & Govedarica, M. (2024). Detection of hyperbolic reflections on real GPR data using YOLO model trained with synthetic data. In *2024 47th international conference on telecommunications and signal processing (TSP)* (pp. 40–44). IEEE.

Cha, Y. J., Choi, W., & Büyüköztürk, O. (2017). Deep learning-based crack damage detection using convolutional neural networks. *Computer-Aided Civil and Infrastructure Engineering, 32*(5), 361–378.

Cha, Y. J., Choi, W., Suh, G., Mahmoudkhani, S., & Büyüköztürk, O. (2018). Autonomous structural visual inspection using region-based deep learning for detecting multiple damage types. *Computer-Aided Civil and Infrastructure Engineering, 33*(9), 731–747.

Chen, X. X., Jiang, H., Xiang, D., Yang, H., & Jiang, Z. S. (2025). RCYOLO: An innovative surface defect detection model for magnetic blocks integrating RevCol and Yolov8s. *Nondestructive Testing and Evaluation, 40*(8), 3493–3516.

Chu, H. H., Long, L. Z., Guo, J. J., Yuan, H. Q., & Deng, L. (2024). Implicit function-based continuous representation for meticulous segmentation of cracks from high-resolution images. *Computer-Aided Civil and Infrastructure Engineering, 39*(4), 539–558.

Chun, P. J., Suzuki, M., & Kato, Y. (2023). Iterative application of generative adversarial networks for improved buried pipe detection from images obtained by ground-penetrating radar. *Computer-Aided Civil and Infrastructure Engineering, 38*(17), 2472–2490.

Diamanti, N., & Redman, D. (2012). Field observations and numerical models of GPR response from vertical pavement cracks. *Journal of Applied Geophysics, 81*, 106–116.

Du, Z. Y., Yuan, J., & Xiao, F. P. (2021). Application of image technology on pavement distress detection: A review. Measurement,184,109900. *Hettiarachchi, 184*, Article 109900.

Fan, J. W., Zhang, Y. M., Ma, T., Zhang, W. G., Zhu, Y. J., & Cheng, H. L. (2024). Permittivity heterogeneity influence of multiphase pavement materials on ground-penetrating radar detection results: A study based on probability distribution. *Journal of Materials in Civil Engineering, 36*(11), Article 04024347.

Fernandes, F. M., & Pais, J. C. (2017). Virtual special issue ground-penetrating radar and complementary non-destructive testing techniques in Civil Engineering laboratory observation of cracks in road pavements with GPR. *Construction and Building Materials, 154*, 1130–1138.

Franesqui, M. A., Yepes, J., & Garcia-Gonzalez, C. (2017). Ultrasound data for laboratory calibration of an analytical model to calculate crack depth on asphalt pavements. *Data in brief, 13*, 723–730.

Guo, X. G., & Wang, N. (2023). Recognition of Pavement Structural Damage Based on Nondestructive Testing and Computer Vision. ASCE International Conference. In *on Computing in Civil Engineering (I3CE)* (pp. 865–873). Corvallis, OR: Oregon State Univ.

Hou, Y., Zhang, Q., Zhao, Z., Zhu, Z., & Zhang, X. (2025). YOLOv5s-MRD:Efficient fire and smoke detection algorithm for complex scenarios based on YOLOv5s. *Journal of Computer Applications, 45*(4), 1317–1324.

Huang, Z. Y., Xu, G. Y., Zhang, X. N., Zang, B., & Yu, H. Y. (2025). Three-dimensional ground-penetrating radar-based feature point tensor voting for semi-rigid base asphalt pavement crack detection. *Developments in the Built Environment, 21*.

Krysinski, L., & Sudyka, J. (2013). GPR abilities in investigation of the pavement transversal cracks. *Journal of Applied Geophysics, 97*, 27–36.

Lahnsteiner, L., Grössbacher, D., Bürger, M., & Zauner, G. (2024). Automatic object detection in radargrams of multi-antenna GPR systems based on simulation data for railway infrastructure analysis. *Applied Sciences-Basel, 14*(8).

Levatti, H. U., Prat, P. C., Ledesma, A., Cuadrado, A., & Cordero, J. A. (2017). Experimental analysis of 3D cracking in drying soils using ground-penetrating radar. *Geotechnical Testing Journal, 40*(2).

Li, B. L., Qi, Y., Fan, J. S., Liu, Y. F., & Liu, C. (2023). A grid-based classification and box-based detection fusion model for asphalt pavement crack. *Computer-Aided Civil and Infrastructure Engineering, 38*(16), 2279–2299.

Li, Y. S., Liu, C. L., Yue, G. H., Gao, Q., & Du, Y. C. (2022). Deep learning-based pavement subsurface distress detection via ground penetrating radar data. *Automation in Construction, 142*.

Liang, X. M., Yu, X., Chen, C., Jin, Y., & Huang, J. D. (2022). Automatic classification of pavement distress using 3D ground-penetrating radar and deep convolutional neural network. *IEEE Transactions on Intelligent Transportation Systems, 23*(11), 22269–22277.

Lin, X., Zhang, J., Wu, D. F., Meng, E. H., Liu, M. Y., Li, M., & Gao, F. L. (2023). Intelligent identification of pavement cracks based on PSA-net. *Frontiers in Environmental Science, 11*.

Liu, W. B., Yang, X., Yan, Y. X., Wang, H. N., Zhang, J. Q., & Heikkilä, R. (2025). A state-of-the-art review on graph characterization and automated detection of road underground targets using ground-penetrating radar. *Measurement, 244*.

Liu, Z., Gu, X. Y., Chen, J. Q., Wang, D. Y., Chen, Y. H., & Wang, L. T. (2023). Automatic recognition of pavement cracks from combined GPR B-scan and C-scan images using multiscale feature fusion deep neural networks. *Automation in Construction, 146*.

Liu, Z., Gu, X. Y., Li, J., Dong, Q., & Jiang, J. W. (2024). Deep learning-enhanced numerical simulation of ground penetrating radar and image detection of road cracks. *Chinese Journal of Geophysics-Chinese Edition, 67*(6), 2455–2471.

Liu, Z., Gu, X. Y., Wu, W. X., Zou, X. Y., Dong, Q., & Wang, L. T. (2022). GPR-based detection of internal cracks in asphalt pavement: A combination method of DeepAugment data and object detection. *Measurement, 197*.

Malek, K., Mohammadkhorasani, A., & Moreu, F. (2023). Methodology to integrate augmented reality and pattern recognition for crack detection. *Computer-Aided Civil and Infrastructure Engineering, 38*(8), 1000–1019.

Niu, W., & Yin, M. (2023). Road small target detection algorithm based on improved YOLO v5. *Chinese Journal of Sensors and Actuators, 36*(1), 36–44.

Rasol, M. A., Pérez-Gracia, V., Solla, M., Pais, J. C., Fernandes, F. M., & Santos, C. (2020). An experimental and numerical approach to combine Ground Penetrating Radar and computational modeling for the identification of early cracking in cement concrete pavements. *Ndt & E International, 115*.

Tavassoti, P., Ameen, T. H., Baaj, H., & Cascante, G. (2022). Novel analysis of ultrasonic pulse propagation tests for characterization of asphalt concrete. *Journal of Testing and Evaluation, 50*(2), 889–904.

Tong, Z., Gao, J., Han, Z. Q., & Wang, Z. J. (2018). Recognition of asphalt pavement crack length using deep convolutional neural networks. *Road Materials and Pavement Design, 19*(6), 1334–1349.

Tong, Z., Gao, J., & Zhang, H. T. (2017). Recognition, location, measurement, and 3D reconstruction of concealed cracks using convolutional neural networks. *Construction and Building Materials, 146*, 775–787.

Torbaghan, M. E., Li, W. D., Metje, N., Burrow, M., Chapman, D. N., & Rogers, C. D. F. (2020). Automated detection of cracks in roads using ground penetrating radar. *Journal of Applied Geophysics, 179*.

Wen, Y. T., Cheng, J. X., Ren, Y. X., Feng, Y. K., Zhang, Z. W., & Zhang, Y. Y. (2024). Complex defects detection of 3-D-printed lattice structures: Accuracy and scale improvement in YOLO V7. *IEEE Transactions on Instrumentation and Measurement, 73*.

Xiong, X., Tan, Y., Tang, J., & Deng, H. (2023). Rapid recognition of asphalt pavement internal diseases based on ground penetrating radar. *Journal of Huazhong University of Science and Technology. Nature Science, 51*(11), 120–127.

Xiong, X. T., Meng, A. X., Lu, J., Tan, Y. Q., Chen, B., Tang, J. M., Zhang, C., Xiao, S. Q., & Hu, J. Y. (2024). Automatic detection and location of pavement internal distresses from ground penetrating radar images based on deep learning. *Construction and Building Materials, 411*.

Xu, Z. J., Yu, X., Liu, Z., Zhang, S., Sun, Q. X., Chen, N., Lv, H. T., Wang, D. W., & Hou, Y. (2023). Safety Monitoring of Transportation Infrastructure Foundation: Intelligent recognition of subgrade distresses based on B-scan GPR images. *IEEE Transactions on Intelligent Transportation Systems, 24*(12), 15468–15477.

Zhang, B., Cheng, H. Y., Zhong, Y. H., Tao, X. H., Li, G. H., & Xu, S. J. (2023). Automatic quantitative recognition method for vertical concealed cracks in asphalt pavement based on feature pixel points and 3D reconstructions. *Measurement, 220*.

Zhang, W. G., Akber, M. A., Hou, S. G., Bian, J., Zhang, D., & Le, Q. Q. (2019). Detection of dynamic modulus and crack properties of asphalt pavement using a non-destructive ultrasonic wave method. *Applied Sciences-Basel, 9*(15).

Zhu, H. R., Wei, G. F., Ma, D. S., Yu, X., & Dong, C. (2025). Research on the detection and identification method of internal cracks in semi-rigid base asphalt pavement based on three-dimensional ground penetrating radar. *Measurement, 417*.